

Revisiting the zero-temperature phase diagram of stoichiometric SrCoO₃ with first-principles methods

Pablo Rivero

Center for Computation and Technology, Louisiana State University, Baton Rouge, Louisiana 70803, USA

Claudio Cazorla*

School of Materials Science and Engineering, UNSW Australia, Sydney NSW 2052, Australia
Integrated Materials Design Centre, UNSW Australia, Sydney NSW 2052, Australia

By using first-principles methods based on density functional theory we revisited the zero-temperature phase diagram of stoichiometric SrCoO₃, a ferromagnetic metallic perovskite that undergoes significant structural, electronic, and magnetic changes as its content of oxygen is decreased. We considered both bulk and epitaxial thin film geometries. In the bulk case, we found that a tetragonal $P4/mbm$ phase with moderate Jahn-Teller distortions and c/a ratio of $\sim 1/\sqrt{2}$ is consistently predicted to have a lower energy than the thus far assumed ground-state cubic $Pm\bar{3}m$ phase. In thin films, we found two phase transitions occurring at compressive and tensile epitaxial strains. However, in contrast to previous theoretical predictions, our results show that: (i) the phase transition induced by tensile strain is isostructural and involves only a change in magnetic spin order (that is, not a metallic to insulator transformation), and (ii) the phase transition induced by compressive strain comprises simultaneous structural, electronic and magnetic spin order changes, but the required epitaxial stress is so large ($< -6\%$) that is unlikely to be observed in practice. Our findings call for a revision of the crystallographic analysis performed in fully oxidised SrCoO₃ samples at low temperatures, as well as of previous first-principles studies.

PACS numbers: 77.55.Nv, 61.50.Ks, 68.65.Cd, 77.80.bn

I. INTRODUCTION

Oxide perovskites with the general formula ABO₃, in which A and B denote different cations, can undergo abrupt structural, magnetic, and electronic changes upon application of small external fields (e. g., electric, magnetic, and mechanical) and variation of temperature [1–10]. This singular reactivity converts oxide perovskites in excellent candidate materials for developing new information storage and energy conversion technologies. One illustrative example is the design of spintronic devices, in which spin-polarised electric currents are generated with electromagnetic fields or through spin-injection from a ferromagnetic material, in order to exploit the magnetic degree of freedom of electrons [11–13]. In this latter context, ferromagnetic metallic perovskites appear to be especially valuable as they can be employed directly as electrodes in complex oxide heterostructures.

SrCoO_{*x*} is a ferromagnetic metallic perovskite in which significant structural, electronic, and magnetic order changes occur as its content of oxygen is varied ($2.5 \leq x \leq 3.0$) [14, 15]. In stoichiometric samples ($x = 3.0$) the crystalline phase that has been repeatedly reported as the ground state is the perovskite $Pm\bar{3}m$ structure, which exhibits ferromagnetic (FM) spin order at temperatures below $T_C = 280 - 305$ K [16–18]. Experiments and theoretical calculations have assuredly shown that SrCoO₃ possesses an intermediate spin (IS) state with

a magnetic moment of $\sim 2.6\mu_B$ per Co ion [18–21]. In non-stoichiometric samples with high oxygen deficiency ($x = 2.5$) the system adopts the brownmillerite phase, which presents atomically ordered one-dimensional vacancy channels and antiferromagnetic (A) spin order at temperatures below $T_C = 570$ K [22–24].

Recently, it has been shown that the content of oxygen in SrCoO_{*x*} thin films can be effectively tuned by means of epitaxial strain [14, 15, 25–28]. This control of oxygen non-stoichiometry offers a promising new route for designing multifunctional oxide materials with improved electrochemical, magnetoresistance, and catalytic properties. Interestingly, Lee and Rabe have identified SrCoO₃ thin films as good candidate materials in which to observe large magnetoelectric effects, that is, a strong coupling between polar and magnetic degrees of freedom, based on the results of first-principles density functional theory (DFT) calculations [29, 30]. Specifically, it has been predicted that simultaneous magnetic-ferroelectric and metal-insulator transitions could be induced in SrCoO₃ by means of moderate tensile and compressive epitaxial strains. If confirmed, these results could advance the development of low-power high-efficiency electronic and energy conversion technologies.

Here, we present a revision of the zero-temperature phase diagram of stoichiometric SrCoO₃ (SCO), both in bulk and thin film geometries, using a wide variety of first-principles DFT techniques (i. e., LDA+U, GGA+U and hybrid exchange-correlation functionals). Our computational analysis consistently shows that, rather than the well-known cubic $Pm\bar{3}m$ phase, a tetragonal $P4/mbm$ phase with moderate Jahn-Teller distortions

*Corresponding Author

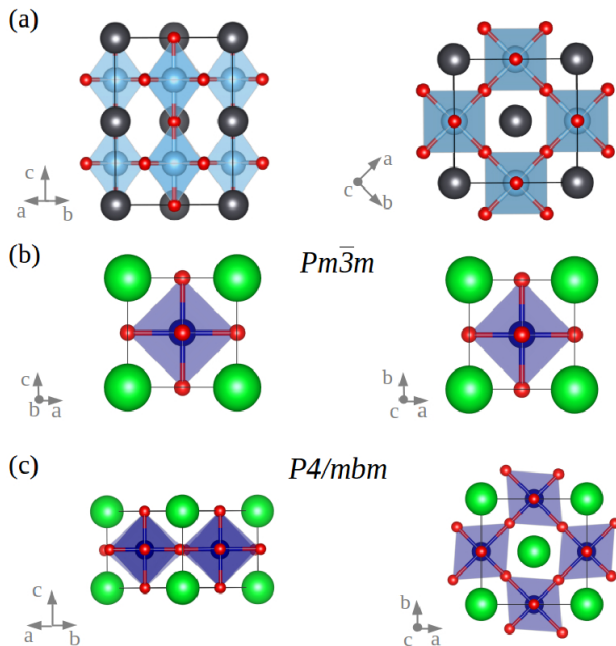


FIG. 1: (a) Sketch of the 20-atom $\sqrt{2} \times \sqrt{2} \times 2$ simulation cell used in most of our calculations; black, blue, and red spheres represent A, B, and O atoms in ABO_3 perovskites. The corresponding lattice vectors are $\mathbf{a}_1 = (a, a, 0)$, $\mathbf{a}_2 = (a, -a, 0)$, and $\mathbf{a}_3 = (0, 0, 2a)$, where a is the lattice parameter of the 5-atom primitive perovskite cell. (b) Sketch of the cubic $Pm\bar{3}m$ phase. (c) Sketch of the tetragonal $P4/mbm$ phase. Sr, Co, and O atoms are represented with green, blue, and red spheres, respectively.

tions and a c/a ratio of $\sim 1/\sqrt{2}$ is the energetically most favorable phase in bulk SCO at zero temperature. We arrived at the same conclusion also when considering the application of hydrostatic pressures of up to 70 GPa. This central outcome either calls for a revision of previous crystallographic analysis performed in SCO at low temperatures, or well it represents a failure of DFT methods in describing the competition among crystalline phases in this highly correlated material. We have also investigated the energy, magnetic, and electronic properties of SCO thin films in a wide interval of epitaxial strains, $-7\% \leq \eta \leq +5\%$ ($\eta \equiv (a - a_0)/a_0$, where a_0 is the in-plane equilibrium distance between cations of the same species), using computational techniques similar to those employed by Lee and Rabe (i. e., DFT GGA+U) [29, 30]. Our results show a phase-transition scenario that is compatible with recent experimental observations but appreciably different from the one proposed previously. Actually, our findings lower the expectations of realising large magnetoelectricity in stoichiometric SCO thin films.

The organisation of this article is as it follows. In the following section we provide an overview of the computational methods employed in this study. Next, we present our results along with some discussion. Finally, we summarise our main findings in Sec. IV.

II. COMPUTATIONAL METHODS

In order to accurately describe the physical properties of $SrCoO_3$ it is necessary to use methods that go beyond standard DFT, e. g., GGA+U (or LDA+U) and hybrid functionals, as due to the presence of strongly correlated d electrons. The GGA+U approximation is based on a Hubbard-type Hamiltonian approach in which an on-site constant effective potential is introduced to account for the intra-atomic electron Coulomb repulsive (J_1) and intra-orbital exchange potential (J_2) [31]. Here we employ the GGA+U (and LDA+U) scheme due to Dudarev [32] for a better treatment of Co's $3d$ electrons; the meaningful term in this approach is $U_{eff} \equiv J_1 - J_2$, to which we refer hereafter simply as to U . The choice of the U value, however, is not unique or rigorously well defined. In general, this is selected so as to reproduce a particular set of experimental data (e. g., lattice parameters or energy band gaps) or theoretical results obtained with higher accuracy methods as closely as possible [33–35].

Hybrid functionals represent a good alternative to DFT+U approximations. In this context, one mixes a particular amount of nonlocal Hartree-Fock (HF) exchange, α , with standard density functional (either LDA or GGA) exchange potentials. The resulting hybrid DFT exchange-correlation potential can be expressed as:

$$V_{xc}^{hybrid} = \alpha V_x^{HF} + (1-\alpha)V_x^{GGA/LDA} + V_c^{GGA/LDA}, \quad (1)$$

where V_x and V_c represent exchange and correlation functionals, respectively. In contrast to GGA+U and LDA+U, hybrid functionals account for both the electronic localisation acting on all the states of the system and nonlocal exchange effects. Yet, in a strict *ab initio* sense, there is not a general prescription for choosing the right amount of nonlocal HF exchange.

In this work, we have used both the GGA+U (LDA+U) and hybrid functional approaches. Next, we explain the technical details of our calculations.

A. GGA+U calculations

In most of our calculations we used the generalised gradient approximation to density functional theory (DFT) proposed by Perdew, Burke, and Ernzerhof (PBE) [36], as it is implemented in the VASP package [37]. Other common exchange-correlation functional approximations such as LDA [38] and PBE^{sol} [39] were also considered. We used the “projector augmented wave” method to represent the ionic cores [40], considering the following electrons as valence states: Co's $3p$, $3d$, and $4s$; Sr's $4s$, $5s$, and $4p$; and O's $2s$ and $2p$. The wave functions were expanded in a plane-wave basis truncated at 500 eV, and a $\sqrt{2} \times \sqrt{2} \times 2$ simulation cell containing up to 20 atoms was used in most of our energy and geometry relaxation calculations (see Fig. 1a). For integrations in the Brillouin zone (BZ), we employed Γ -centered q-point grids

of $8 \times 8 \times 8$. Using these parameters we obtained enthalpy energies that were converged to within 0.5 meV per formula unit (f.u.). Geometry relaxations were performed using a conjugate-gradient algorithm that varied the shape and in some cases also the volume of the unit cell; the imposed tolerance on the atomic forces was $0.01 \text{ eV} \cdot \text{\AA}^{-1}$. High-pressure equations of state were determined by computing the total energy of the crystal in a series of volume points that subsequently were fitted to analytical Birch-Murnaghan functions [41].

We also calculated the vibrational phonon spectrum of several bulk phases by using the “direct method” [42, 43] and DFT calculations. In the direct method, the force-constant matrix of the crystal is calculated in real-space by considering the proportionality between atomic displacements and forces when the former are sufficiently small. Large supercells need to be constructed in order to guarantee that the elements of the force-constant matrix have all fallen off to negligible values at their boundaries, a condition that follows from the use of periodic boundary conditions [44]. Once the force-constant matrix is calculated one can Fourier-transform it to obtain the phonon spectrum at any \mathbf{q} -point. The quantities with respect to which our phonon calculations need to be converged are the size of the supercell, the size of the atomic displacements, and the numerical accuracy in the sampling of the Brillouin zone. We found the following settings to provide zero-point energies [10] converged to within 5 meV/f.u.: $2 \times 2 \times 2$ supercells containing up to 160 atoms, atomic displacements of 0.02 \AA , and \mathbf{q} -point grids of $12 \times 12 \times 12$. The value of the phonon frequencies were obtained with the PHON code developed by Alfé [44]. In using this code we exploited the translational invariance of the system to impose the three acoustic branches to be exactly zero at the Γ \mathbf{q} -point, and used central differences in the atomic forces (i. e., positive and negative atomic displacements were considered).

B. Hybrid functional calculations

Hybrid functional DFT calculations were performed with the replicated-data version of the CRYSTAL14 package [45]. This is a first-principles electronic structure software which employs atom-centered Gaussian-type orbital (GTO) basis sets to build Bloch functions that represent the one-electron crystalline orbitals. GTO offer a number of convenient computational features, e. g., the use of local basis sets containing minimal overlap with neighboring orbitals, that allow to perform HF exchange calculations in medium and large size systems affordably (e. g., the resulting computational expense scales as N^{2-3} with the number of particles, to be compared with the usual N^4 scaling found in plane-waves based methods). All-electron GTO atomic basis sets were chosen as it follows: for Co’s we used the double-zeta all-electron basis set from [46]; for Sr’s small-core Hay-Wadt pseudopotentials [47] were adopted for the description of the

inner-shell electrons $1s$, $2s$, $2p$, $3s$, $3p$, and $3d$, while for the valence part $4s$, $4p$, and $5s$ we used the optimized basis set successfully applied to the strontium titanate study [48]; and for O’s we used the $8 - 411d$ all-electron basis set constructed by Corà [49].

A Monkhorst-Pack $8 \times 8 \times 8$ \mathbf{q} -point grid was used for BZ sampling. The thresholds controlling the accuracy in the calculation of the Coulomb and exchange integrals were set equal to 10^{-7} and 10^{-14} , and to 10^{-7} eV in the SCF energy. The crystal cell parameters and atomic positions were relaxed during the geometry optimisations by imposing a convergence criterion of $0.008 \text{ eV} \cdot \text{\AA}^{-1}$ in the atomic forces. The hybrid functionals employed in this study include PBE-10 [35], PBE0 [50], and HSE06 [51]. In the first two versions, the amount of HF exchange is 0.10 and 0.25, respectively (that is, parameter α in Eq. 1); in the HSE06 case, there is a separation between short and long ranges in which $\alpha = 0.25$ and 1.00 are used, respectively.

III. RESULTS AND DISCUSSION

A. Intermediate spin state and the choice of U

There is strong experimental and theoretical evidence showing that bulk SCO possesses an intermediate spin (IS) state resulting from a competition between intra-atomic exchange interactions and the crystal field [18–21]. This IS configuration can be understood as a high spin state in the Co^{3+} ions that is antiferromagnetically coupled to a ligand hole of e_g symmetry, which can be formally represented with the d -orbital occupation model $t_{2g}^4 e_g^1$ (see Fig. 2a) [19, 21]. In Fig. 2b, we show the partial density of electronic d states (pDOS) calculated in bulk SCO in the cubic $Pm\bar{3}m$ phase with the hybrid functional PBE-10 (see Fig. 1b); our hybrid functional pDOS results reproduce the expected orbital occupation configuration $t_{2g}^4 e_g^1$: two unoccupied t_{2g}^\downarrow states (d_{xz} and d_{yz} above the Fermi energy level, E_F) and one occupied t_{2g}^\uparrow state (d_{xy} below E_F), while e_g states are smeared over a large energy range containing E_F in the spin-up channel.

In Fig. 3, we show the d -orbital pDOS calculated also in bulk SCO considering the cubic $Pm\bar{3}m$ phase but employing the GGA+U method. Several U values were employed in order to analyse the effect of this term on the description of the expected IS state. It is found that only for $U > 5$ eV the IS state in bulk SCO is reproduced correctly, as otherwise a low spin state is obtained (that is, no particular d state is unoccupied). For instance, in the $U = 6$ eV case the two unoccupied t_{2g}^\downarrow states (d_{xz} and d_{yz} above E_F) are properly rendered whereas in the $U = 2$ and 4 eV cases those appear as partially occupied. We note that these conclusions are in agreement with recent results reported by Hoffmann *et al.* in work [21]. In view of these findings, we adopted $U = 6$ eV for

	ΔE (meV/f.u.)	M (μ_B)	a (Å)	b (Å)	c (Å)	x	Q_2 (Å)	Q_3 (Å)
HSE06	-632	2.53	5.429	5.429	3.912	0.272	0.474	0.060
PBE0	-269	2.50	5.424	5.424	3.909	0.227	0.498	0.060
PBE - 10	-259	2.28	5.392	5.392	3.979	0.233	0.376	0.136
PBE + U	-126	2.84	5.502	5.502	3.943	0.268	0.397	0.042
PBE ^{sol} + U	-117	2.78	5.404	5.404	3.873	0.266	0.345	0.042
LDA + U	-109	2.86	5.313	5.313	3.811	0.265	0.324	0.044

TABLE I: Energy, structural, and magnetic properties of bulk equilibrium SrCoO₃ calculated in the tetragonal $P4/mbm$ phase using several hybrid and DFT functionals ($U = 6$ eV). $\Delta E \equiv E(P4/mbm) - E(Pm\bar{3}m)$, M is the magnetic moment per Co ion, a , b , c , the length of the lattice vectors, x the displacement of the equatorial O atoms sitting in h Wyckoff positions, and Q_2 and Q_3 lattice Jahn-Teller distortion parameters (see text).

the rest of our GGA+U (and LDA+U) calculations. It is worth noticing that in previous GGA+U studies by Lee and Rabe [29, 30] $U < 5$ eV values were employed, hence the d -orbital configurations sampled therein are likely to differ from the expected IS state.

B. Bulk SrCoO₃ at equilibrium

In all our GGA+U, LDA+U and hybrid functional DFT calculations, we consistently found that a tetragonal $P4/mbm$ phase displaying moderate Jahn-Teller distortions and a c/a ratio of $\sim 1/\sqrt{2}$ (see Fig. 1c) has a lower energy than the cubic $Pm\bar{3}m$ phase, thus far assumed to be the ground-state in bulk SCO [16–18]. In particular, the new tetragonal $P4/mbm$ phase (space group 127) has a 10-atoms unit cell in which two Co atoms site on c Wyckoff positions, two Sr atoms on a Wyckoff positions, two apical O atoms on d Wyckoff positions, and four equatorial O atoms on h Wyckoff positions. The Jahn-Teller (JT) distortions that are relevant to this structure can be expressed as:

$$Q_2 = \frac{2(l-s)}{\sqrt{2}}, \quad (2)$$

$$Q_3 = \frac{2(2m-l-s)}{\sqrt{6}}, \quad (3)$$

where l , m , and s refer to the long, medium and short Co-O distances, respectively (see Fig. 4). A third possible JT distortion associated to a breathing mode, Q_1 (see Fig. 4), was found to be negligible in bulk SCO.

In Table I, we summarise our energy, structural, and magnetic results obtained in the new tetragonal $P4/mbm$ phase. As it is appreciated therein, the energy difference between the tetragonal $P4/mbm$ and cubic $Pm\bar{3}m$ phases, $\Delta E \equiv E(P4/mbm) - E(Pm\bar{3}m)$, is of the order of ~ 0.1 eV/f.u., that is, fairly large, with hybrid

functionals providing the largest $|\Delta E|$ values. In most cases the predicted magnetic moment per Co ion is of $2.5 - 2.9\mu_B$, which is consistent with the expected intermediate spin state [18–21]. Regarding the structural features, all DFT functionals render a c/a ratio of $\sim 1/\sqrt{2}$, which denotes very small tetragonality as the unit cell of the $P4/mbm$ phase can be thought of a $\sqrt{2} \times \sqrt{2} \times 1$ supercell constructed with the usual 5-atom perovskite unit cell. The x displacement associated to h Wyckoff positions, which are occupied by equatorial oxygen atoms, varies from 0.23 to 0.27 depending on the employed functional. Finally, the Q_2 JT distortion, which mostly affects to the equatorial plane in the oxygen octahedra (see Fig. 4), appears to be the dominant one.

We have calculated the d -orbital pDOS of bulk SCO in the new tetragonal $P4/mbm$ phase with the hybrid functional PBE-10 (see Fig. 5b). Our results reproduce the expected orbital occupation configuration $t_{2g}^4 e_g^1$: two unoccupied t_{2g}^\downarrow states (d_{xy} and d_{yz}/d_{xz} above E_F) and one occupied t_{2g}^\downarrow state (d_{yz}/d_{xz} below E_F), while e_g states are smeared over a large energy range containing E_F in the spin-up channel. The main effect deriving from the presence of JT distortions and lowering of crystal symmetry as compared to the cubic $Pm\bar{3}m$ phase, is to swap the energy ordering between t_{2g} d -states (see Figs. 2a and 5a). Analogous d -orbital pDOS results were obtained also with the PBE+U method.

We calculated the lattice phonon spectrum of bulk SCO in the new tetragonal $P4/mbm$ phase with the PBE+U method. It was found that this structure is vibrationally and mechanically stable as none imaginary phonon frequency appeared in the corresponding Brillouin zone (see Fig. 6). Interestingly, we performed analogous phonon calculations in the cubic $Pm\bar{3}m$ phase and found few imaginary phonon frequencies at the high-symmetry reciprocal-space point $M = (\frac{1}{2}\frac{1}{2}0)$. This finding is consistent with the fact that by enlarging the 5-atom perovskite unit cell along the $x-y$ Cartesian direc-

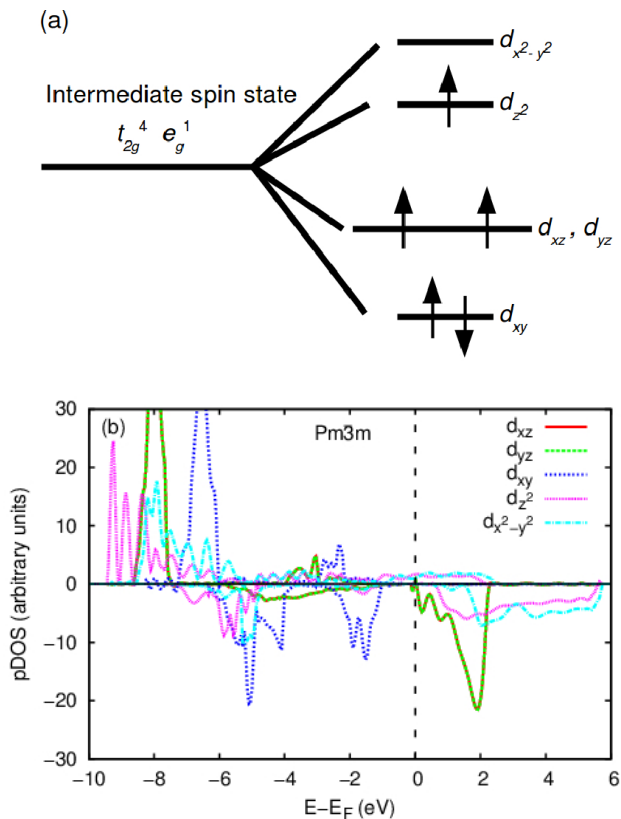


FIG. 2: (a) Sketch of a possible intermediate spin state expected to occur in bulk SrCoO_3 [19]. (b) Density of electronic d states calculated for bulk SrCoO_3 in a cubic $Pm\bar{3}m$ phase with the PBE+U hybrid functional. Spin-up and spin-down electronic densities are represented with positive and negative values, respectively.

tions it is possible to find a lower-energy crystal structure at zero temperature. Also, it suggests that SCO in the cubic $Pm\bar{3}m$ phase may be highly anharmonic. Consequently, at $T \neq 0$ K conditions, the cubic $Pm\bar{3}m$ phase could be entropically stabilised over the tetragonal $P4/m\bar{b}m$ phase [52, 53]; such a possibility, however, has not been explored in this work.

C. Bulk SrCoO_3 under pressure

Under compression, oxide perovskites may undergo phase transformations into higher symmetry configurations [54, 55]. For this reason, we analysed the possibility of a P -induced $P4/m\bar{b}m \rightarrow Pm\bar{3}m$ phase transition in bulk SCO with the PBE+U method. In Fig. 7a, we show the zero-temperature enthalpy difference calculated between the two phases, $\Delta H \equiv H(P4/m\bar{b}m) - H(Pm\bar{3}m)$, expressed as a function of pressure. As it is observed therein, the effect of compression initially is to reduce the value of $|\Delta H|$, however, at $P > 45$ GPa this trend is reverted. Such a change of tendency is due to the disap-

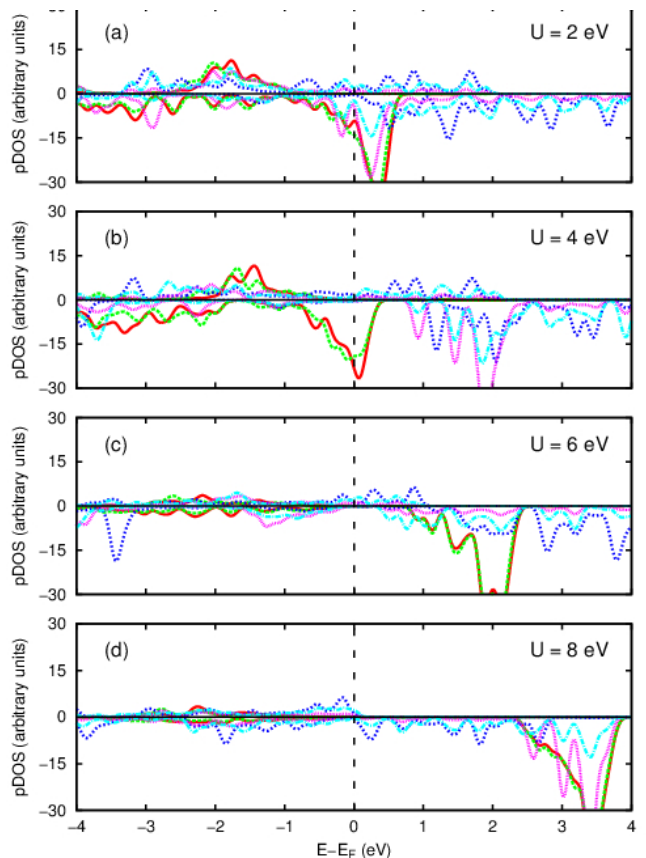


FIG. 3: Density of electronic d states calculated in bulk SrCoO_3 in the cubic $Pm\bar{3}m$ phase with the PBE+U method expressed as a function of U . Spin-up and spin-down electronic densities are represented with positive and negative values, respectively. The convention in representing the d states is the same than in the previous figure. U values smaller than 5 eV do not reproduce the expected intermediate spin state in bulk SCO.

pearance of an energy band gap in the spin-down channel of the cubic $Pm\bar{3}m$ phase (not shown here); the d -orbital pDOS estimated in the tetragonal $P4/m\bar{b}m$ phase, on the contrary, always displays an intermediate spin state in the interval $0 \leq P \leq 70$ GPa.

In a recent experimental study on bulk SCO at $T = 200$ K, Yang *et al.* have reported two P -induced phase transitions occurring at $P \sim 1$ and ~ 45 GPa and involving a spin reorientation and spin-state change, respectively [56]. These observations are not coincident with our results obtained in bulk stoichiometric SCO. The reasons behind such a disagreement could be explained in terms of (i) the neglect of thermal excitations in our theoretical study, and/or (ii) the presence of small oxygen deficiencies in the experimental samples (i. e., $\text{SrCoO}_{3-\delta}$ with $\delta = 0.05$, as reported by Yang *et al.* [56]). In order to substantiate the effects of small non-stoichiometry in bulk SCO under pressure (at zero temperature), we calculated the enthalpy of $\text{SrCoO}_{2.75}$ crystals (that is, generated by removing one oxygen atom

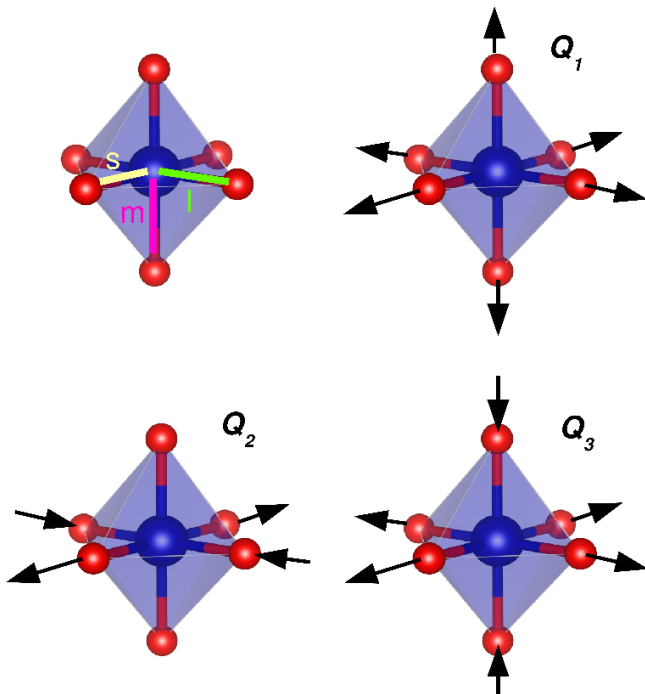


FIG. 4: Sketch of possible Jahn-Teller distortion modes in SrCoO_3 and of the distorted Co-O bonds l , m , and s .

from the stoichiometric 20-atoms unit cell) as a function of pressure. We considered four possible magnetic spin arrangements: ferromagnetic (FM), antiferromagnetic A-type (A-A, parallel in-plane spins, antiparallel out-of-plane spins), antiferromagnetic G-type (A-G, antiparallel in-plane spins, antiparallel out-of-plane spins), and antiferromagnetic C-type (A-C, antiparallel in-plane spins, parallel out-of-plane spins).

In Fig. 7b, we plot the zero-temperature enthalpy difference calculated among the lowest-energy $\text{SrCoO}_{2.75}$ configurations obtained when constraining ferromagnetic (FM) and antiferromagnetic A-type (A-A) spin orders, $\Delta H^m \equiv H^{A-A} - H^{FM}$, as those were found to be the energetically most favorable cases. It is observed that at $P \sim 0$ GPa the enthalpy difference ΔH^m adopts very small and positive values, which indicates that FM spin order remains the most stable; however, when pressure is increased beyond 0.75 GPa the system with A-A spin order becomes the ground state. We note that this transition point is very close to the pressure at which Yang *et al.* have observed a reorientation of magnetic spins in SCO (i. e., 1.1 GPa [56]); nevertheless, our calculated ΔH^m values within the pressure interval $0 \leq P \leq 1$ GPa are so small (i. e., of the order of our accuracy threshold of ~ 1 meV/f.u.) that we cannot discard that bulk $\text{SrCoO}_{2.75}$ is already antiferromagnetic close to equilibrium. As pressure is increased beyond 33 GPa, the system displaying FM spin order clearly becomes the one with the lowest energy. According to our calculations, this magnetic spin order phase transformation is accom-

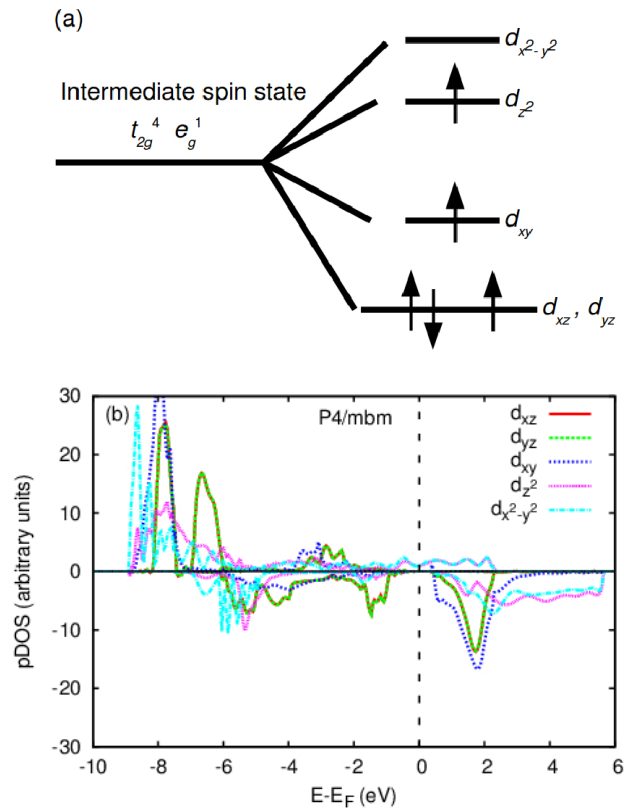


FIG. 5: (a) Sketch of a possible intermediate spin state expected to occur in bulk SrCoO_3 [19]. (b) Density of electronic d states calculated for bulk SrCoO_3 in a tetragonal $P4/mbm$ phase with the PBE-10 hybrid functional. Spin-up and spin-down electronic densities are represented with positive and negative values, respectively.

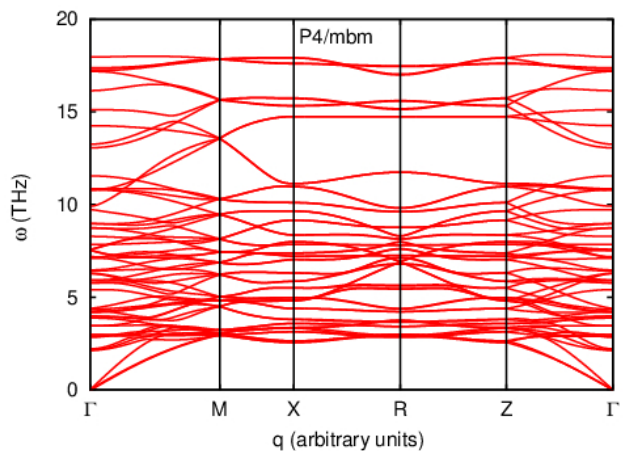


FIG. 6: Lattice phonon spectrum calculated for bulk SrCoO_3 in a tetragonal $P4/mbm$ phase with the PBE+U method ($U = 6$ eV).

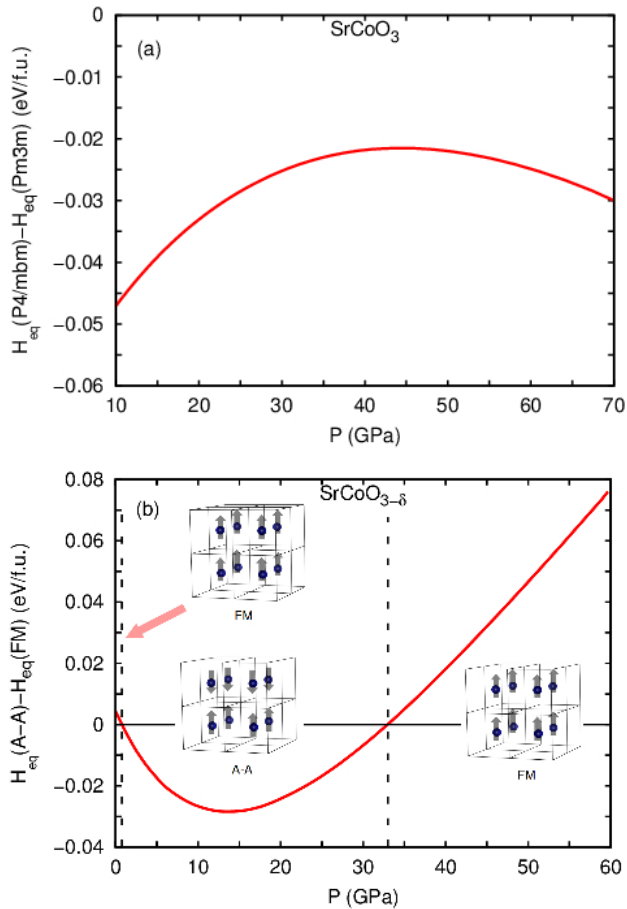


FIG. 7: (a) Enthalpy energy difference between the tetragonal $P4/mbm$ and cubic $Pm\bar{3}m$ phases calculated in stoichiometric SCO as a function of pressure. (b) Enthalpy energy difference between magnetic spin orders A-A and FM calculated in non-stoichiometric SCO ($\text{SrCoO}_{2.75}$) as a function of pressure. The vertical dashed lines indicate P -induced phase transitions affecting the magnetic spin order.

panied by a very small volume reduction of 0.8 %, in which the volume of the A-A phase is 49.15 \AA^3 .

In view of our zero-temperature results obtained in bulk $\text{SrCoO}_{3-\delta}$ under pressure, Yang *et al.*'s observations reported at $P \sim 45$ GPa [56] could be reinterpreted as a full magnetic spin order transformation, rather than as a spin-state change. In fact, the phase transition that we report in $\text{SrCoO}_{2.75}$ is isostructural and continuous, as it has been observed in the laboratory. However, no intermediate to low spin state transition is observed in our calculations, neither in the stoichiometric nor in the non-stoichiometric case, when considering the lowest-energy phases. Further experimental studies in compressed SCO are highly desirable in order to rigorously confirm or reject our hypothesis.

D. SrCoO_3 thin films

Lee and Rabe have recently predicted a series of intriguing multiferroic phase transformation occurring in stoichiometric SCO thin films, based on GGA+U DFT calculations [29, 30]. In particular, it has been proposed that both small tensile and compressive epitaxial strains (i. e., of $\sim +2$ % and ~ -1 %, respectively) can trigger a transformation from the bulk FM-metallic phase into an A-insulating-ferroelectric phase. These theoretical results suggest that large magnetoelectric effects, that is, cross responses to applied electric and magnetic fields, could be realised in SCO thin films, as in regions where several multiferroic phases are energetically competitive those can be expected to happen [57, 58]. In two recent experimental studies on $\text{SrCoO}_{3-\delta}$ thin films by Callori *et al.* [26] and Hu *et al.* [27], the existence of an antiferromagnetic phase at moderate tensile strains of $\sim +2.7$ % has been ascertained; however, the accompanying metal-to-insulator and nonpolar-to-ferroelectric phase transitions as predicted by Lee and Rabe appear to be missing. The second multiferroic phase transformation that has been anticipated to occur at compressive strains also remains experimentally unverified, in spite of the small epitaxial distortions that have been suggested to be involved (i. e., ~ -1 %) [29, 30].

In view of the results presented in previous sections, we considered as opportune to revise the zero-temperature phase diagram of stoichiometric SCO thin films that is obtained with first-principles methods. We employed the PBE+U method with $U = 6$ eV, in order to reproduce the expected intermediate spin state correctly (see Sec. III A). In addition to the tetragonal $P4/mbm$ and cubic $Pm\bar{3}m$ phases considered so far in this study (we note that the latter phase transforms into tetragonal $P4/mmm$ when applying epitaxial strain on it), we analysed many other structures exhibiting tetragonal (e. g., $P4mm$, $P4cc$, and $P4_2/mmm$), orthorhombic (e. g., $Amm2$, $Pna2_1$, and $Pmc2_1$) and monoclinic (e. g., $C2/m$, $P2/m$, and $P2_1/c$) crystalline symmetry. All those structures were considered in the four magnetic spin arrangements that can be reproduced with our 20-atoms simulation cell, namely, FM, A-A, A-C, and A-G (see Sec. III C).

In Fig. 8, we represent the zero-temperature energy of the crystal phases that according to our DFT calculations are energetically most competitive in stoichiometric SCO thin films (some irrelevant magnetic order phases have been omitted for clarity) as a function of epitaxial strain, η [$\equiv (a - a_0)/a_0$, where a_0 is equal to 3.89 \AA]. Interestingly, we found an extreme and complex competition between FM and A-A phases, including tetragonal, orthorhombic and monoclinic crystals, at $\eta \sim 0$ % conditions. In particular, the energy of the orthorhombic $Cmmm$ and monoclinic $C2/m$ and $P2_1/c$ phases, either in the FM or A-A magnetic spin arrangements, are just ~ 20 meV/f.u. above that of the tetragonal $P4/mbm$ phase (FM case). (We note that none of

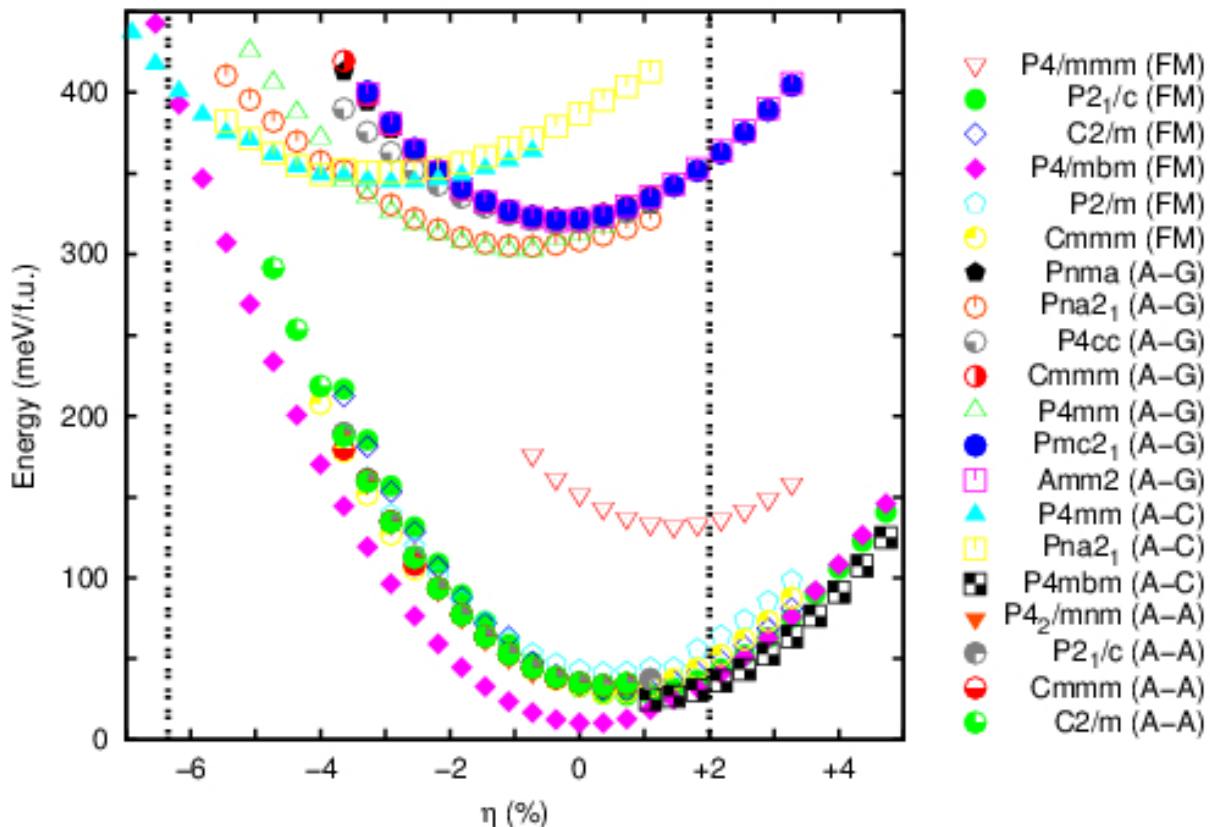


FIG. 8: Energy of several competitive phases in SrCoO₃ thin films calculated as a function of epitaxial strain. The vertical dashed lines indicate η -induced phase transitions affecting the structural, magnetic, and electronic properties of the system.

these low-energy structures was considered by Lee and Rabe in works [29, 30].) Such a fierce phase competition appears to be comparable to that found in archetypal multiferroic compounds like, for instance, BiFeO₃ [59]. Meanwhile, at small epitaxial strain conditions phases displaying A-C and A-G magnetic spin orders are found to be energetically noncompetitive, made the exception of the tetragonal $P4/mbm$ phase (A-C case).

At $\eta = +2\%$, we found that the tetragonal ground-state phase undergoes a magnetic phase transition from FM to A-C (see vertical dashed lines in Fig. 8). This is a continuous and isostructural phase transformation. In order to identify possible electronic-structure changes associated to this transition, we calculated the d -orbital pDOS in the two relevant $P4/mbm$ phases (see Fig. 9). Our results suggest a change from an intermediate spin state in the FM phase to a low spin state in the A-A phase, as in the latter case no energy band gap appears in the spin-down channel. Likewise, along the tensile strain-induced phase transition the system is likely to improve its electrical conductivity properties rather than to become an insulator (in contrast to the $P4/mmm \rightarrow Pmc2_1$ transformation suggested in [29, 30], which renders an insulator and ferroelectric compound at $\eta \sim +3\%$). Our predictions appear to

be consistent with recent experimental observations reported by Callori *et al.* [26] and Hu *et al.* [27]. Nevertheless, new experimental studies characterising in detail the structural and electronic features of SCO thin films at moderate tensile strains appear to be necessary for clarifying the discrepancies found between ours and previous DFT results [29, 30].

At $\eta = -6.4\%$, we found that the system transforms into a tetragonal $P4mm$ phase displaying A-C spin order and a large c/a ratio of ~ 1.3 (see vertical dashed lines in Fig. 8). In order to identify possible electronic-structure changes associated to this transition, we calculated the d -orbital pDOS in the two involved tetragonal phases (see Fig. 10). Our analysis reveals that SCO $P4mm$ (A-C) thin films are insulator and also ferroelectric, in particular they exhibit a large out-of-plane electrical polarisation of $\sim 115 \mu\text{C}/\text{m}^2$ (as it has been estimated with the methods explained in work [60]). The predicted phase transition, therefore, involves a three-fold structural, magnetic, and ferroelectric transformation; however, in spite of its fundamental and technological interests, it requires of so large compressive strains that it would be hardly realisable in practice (in contrast to the multiferroic phase transformation predicted by Lee and Rabe at $\eta \sim -1\%$ [29, 30]). Nonetheless, we found that for the same type of

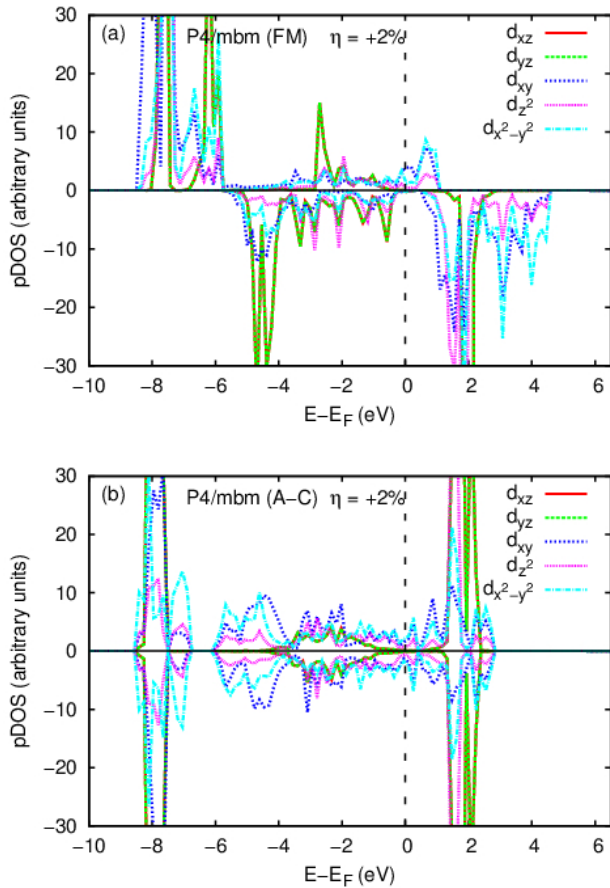


FIG. 9: Density of electronic d states calculated with the PBE+U method ($U = 6$ eV) in tensile SrCoO₃ thin films in the tetragonal (a) $P4/mbm$ [FM] and (b) $P4/mbm$ [A-C] phases. Spin-up and spin-down electronic densities are represented with positive and negative values, respectively.

phase transformation to occur in nonstoichiometric SCO thin films (i. e., SrCoO_{2.75}) a smaller critical epitaxial strain of $\eta = -5.4\%$ is needed. Magnetoelectric effects then are probably more likely to be observed in nonstoichiometric than in stoichiometric SCO samples.

IV. SUMMARY

We have presented a throughout revision of the zero-temperature phase diagram of stoichiometric SrCoO₃ that is obtained with first-principles methods based on density functional theory (i. e., GGA+U and hybrid functionals). In the bulk case, we have identified a tetragonal $P4/mbm$ phase with moderate JT distortions and a c/a ratio of $\sim 1/\sqrt{2}$ as the ground state of the system. The same phase remains the most stable as hydrostatic pressures of up to ~ 70 GPa are applied. This central result either calls for a revision of previous crystallographic analysis performed in SCO at low temperatures, or well

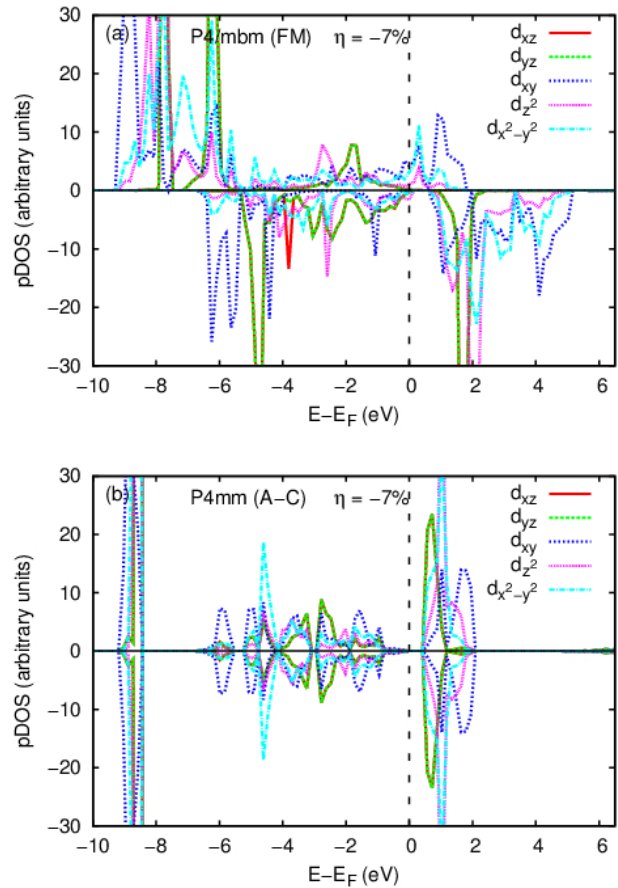


FIG. 10: Density of electronic d states calculated with the PBE+U method ($U = 6$ eV) in highly compressive SrCoO₃ thin films in the tetragonal (a) $P4/mbm$ [FM] and (b) $P4mm$ [A-C] phases. Spin-up and spin-down electronic densities are represented with positive and negative values, respectively.

it represents a failure of DFT methods in describing such a highly correlated oxide compound. In SCO thin films, we have found two phase transitions occurring at moderate tensile and large compressive epitaxial strains (i. e., $\sim +2\%$ and $\sim -6\%$, respectively). According to our calculations, the first transformation is isostructural and comprises only a change in magnetic spin order. The second transition, on the contrary, involves a three-fold structural, magnetic, and polar transformation; however, the critical epitaxial strain associated to this transition is so large that it appears to be unrealisable in practice. The general description of SCO thin films that follows from our study appears to be consistent with recent experimental observations, however, it differs considerably from previously reported DFT GGA+U results. The main reason behind such a disagreement is likely to be related to the choice of the U value, which as we have shown has an important effect on the description of electronic and magnetic spin degrees of freedom. New and systematic experiments on stoichiometric SCO, both in bulk and thin film geometries, certainly are necessary in order to

advance our knowledge of this intriguing material.

Acknowledgments

This research was supported by the Australian Research Council under Future Fellowship funding scheme

(Grant No. FT140100135). Computational resources and technical assistance were provided by the Australian Government through Magnus under the National Computational Merit Allocation Scheme. P. R. acknowledges an allocation of computing time from the Louisiana State University High Performance Computing center.

-
- [1] A. J. Hatt and N. A. Spaldin, *Phys. Rev. B* **82**, 195402 (2010).
- [2] J. M. Rondinelli and N. A. Spaldin, *Adv. Mater.* **23**, 3363 (2011).
- [3] J. M. Rondinelli and S. Coh, *Phys. Rev. Lett.* **106**, 235502(2011).
- [4] S. J. May, J. -W. Kim, J. M. Rondinelli, E. Karapetrova, N. A. Spaldin, A. Bhattacharya, and P. J. Ryan, *Phys. Rev. B* **82**, 014110 (2010).
- [5] C. Cazorla and M. Stengel, *Phys. Rev. B* **90**, 020101(R) (2014).
- [6] C. Cazorla and M. Stengel, *Phys. Rev. B* **92**, 214108 (2015).
- [7] C. W. Swartz and X. Wu, *Phys. Rev. B* **85**, 054102 (2012).
- [8] M. Stengel, C. J. Fennie, and Ph. Ghosez, *Phys. Rev. B* **86**, 094112 (2012).
- [9] J. Hong and D. Vanderbilt, *Phys. Rev. B* **87**, 064104 (2013).
- [10] C. Cazorla and J. Íñiguez, *Phys. Rev. B* **88**, 214430 (2013).
- [11] S. D. Ganichev, E. L. Ivchenko, S. N. Danilov, J. Eroms, W. Wegscheider, D. Weiss, and W. Prettl, *Phys. Rev. Lett.* **86**, 4358 (2001).
- [12] U. Lüders, A. Barthélémy, M. Bibes, K. Bouzehouane, S. Fusil, E. Jacquet, J.-P. Contour, J.-F. Bobo, J. Fontcuberta, and A. Fert, *Adv. Mater.* **18**, 1733 (2006).
- [13] M. Gajek, M. Bibes, S. Fusil, K. Bouzehouane, J. Fontcuberta, A. Barthélémy, and A. Fert, *Nat. Mater.* **6**, 296 (2007).
- [14] H. Jeen, W. S. Choi, M. D. Biegalski, C. M. Folkman, I.-C. Tung, D. D. Fong, J. W. Freeland, D. Shin, H. Ohta, M. F. Chisholm, and H. N. Lee, *Nat. Mater.* **12**, 1057 (2013).
- [15] H. Jeen, W. S. Choi, J. W. Freeland, H. Ohata, C. U. Jung, and H. N. Lee, *Adv. Mater.* **25**, 3651 (2013).
- [16] P. Bezdicka, A. Wattiaux, J. C. Grenier, M. Pouchard, and P. Hagemuller, *Z. Anorg. Allg. Chem.* **619**, 7 (1993).
- [17] S. Kawasaki, M. Takano, and Y. Takeda, *J. Solid State Chem.* **121**, 174 (1996).
- [18] Y. Long, Y. Kaneko, S. Ishiwata, Y. Taguchi, and Y. Tokura, *J. Phys.: Condens. Matt.* **23**, 245601 (2011).
- [19] R. H. Potze, G. A. Sawatzky, and M. Abbate, *Phys. Rev. B* **51**, 11501 (1995).
- [20] M. Zhuang, W. Zhang, A. Hu, and N. Ming, *Phys. Rev. B* **57**, 13655 (1998).
- [21] M. Hoffmann, V. S. Borisov, S. Ostanin, I. Mertig, W. Hergert, and A. Ernst, *Phys. Rev. B* **92**, 094427 (2015).
- [22] T. Takeda, H. Wantanabe, and Y. Yamaguchi, *J. Phys. Soc. Jpn.* **33**, 970 (1972).
- [23] H. Taguchi, M. Shimada, and M. Koizumi, *J. Sol. Stat. Chem.* **29**, 221 (1979).
- [24] C. K. Xie, Y. F. Nie, B. O. Wells, J. I. Budnick, W. A. Hines, and B. Dabrowski, *Appl. Phys. Lett.* **99**, 052503 (2011).
- [25] W. S. Choi, H. Jeen, S. S. A. Seo, V. R. Cooper, K. M. Rabe, and H. N. Lee, *Phys. Rev. Lett.* **111**, 097401 (2013).
- [26] S. J. Callori, S. Hu, J. Bertinshaw, Z. J. Yue, S. Danilkin, X. L. Wang, N. Valanoor, F. Klose, J. Seidel, and C. Ulrich, *Phys. Rev. B* **91**, 140405(R) (2015).
- [27] S. Hu, Z. Yue, J. S. Lim, S. J. Callori, J. Bertinshaw, A. Ikeda-Ohno, T. Ohkochi, C.-H. Yang, X. Wang, C. Ulrich, and J. Seidel, *Adv. Mater. Interfaces* **2**, 1500012 (2015).
- [28] J. R. Petrie, C. Mitra, H. Jeen, W. S. Choi, T. L. Meyer, F. A. Reboredo, J. W. Freeland, G. Eres, and H. N. Lee, *Adv. Funct. Mater.* **26**, 1564 (2016).
- [29] J. H. Lee and K. M. Rabe, *Phys. Rev. Lett.* **107**, 067601 (2011).
- [30] J. H. Lee and K. M. Rabe, *Phys. Rev. B* **84**, 104440 (2011).
- [31] A. I. Liechtenstein, V. I. Anisimov, and J. Zaanen, *Phys. Rev. B* **52**, R5467 (1995).
- [32] S. L. Dudarev, G. A. Botton, S. Y. Savrasov, C. J. Humphreys, and A. P. Sutton, *Phys. Rev. B* **57**, 1505 (1998).
- [33] N. C. Hernández, R. Grau-Crespo, N. H. de Leeuw, and J. F. Sanz, *Phys. Chem. Chem. Phys.* **11**, 5246 (2009).
- [34] J. Hong, A. Stroppa, J. Íñiguez, S. Picozzi, and D. Vanderbilt, *Phys. Rev. B* **85**, 054417 (2012).
- [35] P. Rivero, V. Meunier, and W. Shelton, *Phys. Rev. B* **93**, 024111 (2016).
- [36] J. P. Perdew, K. Burke, and M. Ernzerhof, *Phys. Rev. Lett.* **77**, 3865 (1996).
- [37] G. Kresse and J. Fürthmüller, *Phys. Rev. B* **54**, 11169 (1996); G. Kresse and D. Joubert, *Phys. Rev. B* **59**, 1758 (1999).
- [38] D. M. Ceperley and B. J. Alder, *Phys. Rev. Lett.* **45**, 566 (1980).
- [39] J. P. Perdew, A. Ruzsinszky, G. I. Csonka, O. A. Vydrov, G. E. Scuseria, L. A. Constantin, X. Zhou, and K. Burke, *Phys. Rev. Lett.* **100**, 136406 (2008).
- [40] P. E. Blöchl, *Phys. Rev. B* **50**, 17953 (1994).
- [41] C. Cazorla and J. Boronat, *Phys. Rev. B* **92**, 224113 (2015).
- [42] G. Kresse, J. Furthmüller, and J. Hafner, *Europhys. Lett.* **32**, 729 (1995).
- [43] D. Alfè, G. D. Price, and M. J. Gillan, *Phys. Rev. B* **64**, 045123 (2001).
- [44] D. Alfè, *Comp. Phys. Commun.* **180**, 2622 (2009).
- [45] R. Dovesi, R. Orlando, A. Erba, C. M. Zicovich-Wilson, B. Civalieri, S. Casassa, L. Maschio, M. Ferrabone, M. De

- La Pierre, P. DARco, Y. Noel, M. Causa, M. Rerat, and B. Kirtman, *Int. J. Quantum Chem.* **114**, 1287 (2014).
- [46] <http://www.crystal.unito.it/basis-sets.php>
- [47] P. J. Hay and W. R. Wadt, *J. Chem. Phys.* **82**, 299 (1985).
- [48] S. Piskunov, E. Heifets, R. I. Eglitis, and G. Borstel, *Comput. Mater. Sci.* **29**, 165 (2004).
- [49] F. Corà, *Mol. Phys.* **103**, 2483 (2005).
- [50] C. Adamo and V. Barone, *J. Chem. Phys.* **110**, 6158 (1999).
- [51] A. V. Krukau, O. A. Vydrov, A. F. Izmaylov, and G. E. Scuseria, *J. Chem. Phys.* **125**, 224106 (2006).
- [52] X. Huang, C. Bungaro, V. Godlevsky, and K. M. Rabe, *Phys. Rev. B* **65**, 014108 (2001).
- [53] C. Cazorla, D. Alfè, and M. J. Gillan, *Phys. Rev. B* **85**, 064113 (2012).
- [54] D. Andrault and J. P. Poirier, *Phys. Chem. Minerals* **18**, 91 (1991).
- [55] J. Íñiguez and D. Vanderbilt, *Phys. Rev. Lett.* **89**, 115503 (2002).
- [56] J.-Y. Yang, M. Medarde, J. S. White, D. Sheptyakov, X.-Z. Yan, N.-N. Li, W.-G. Yang, H.-L. Xia, J.-H. Dai, Y.-Y. Yin, Y.-Y. Jiao, J.-G. Cheng, Y.-L. Bu, Q.-F. Zhang, X.-D. Li, C.-Q. Jin, Y. Taguchi, Y. Tokura, and Y.-W. Long, *Phys. Rev. B* **92**, 195147 (2015).
- [57] J. Íñiguez, *Phys. Rev. Lett.* **101**, 117201 (2008).
- [58] J. C. Wojdel and J. Íñiguez, *Phys. Rev. Lett.* **105**, 037208 (2010).
- [59] O. Diéguez, O. E. González-Vázquez, J. C. Wojdel and J. Íñiguez, *Phys. Rev. B* **83**, 094105 (2011).
- [60] C. Cazorla and M. Stengel, *Phys. Rev. B* **92**, 214108 (2015).